ELSEVIER

Journal of Contaminant Hydrology 27 (1997) 83–105

JOURNAL OF
Contaminant
Hydrology

Estimating interfacial areas for multi-fluid soil systems

Scott A. Bradford, Feike J. Leij *

US Salinity Laboratory, US Department of Agriculture, Agricultural Research Service, 450 W. Big Springs Road, Riverside, CA 92507, USA

Received 16 February 1996; revised 4 August 1996; accepted 4 August 1996

Abstract

Knowledge of the fluid–fluid and fluid–solid interfacial areas is important to better understand and quantify many flow and transport processes in porous media. This paper presents estimates for interfacial areas of porous media containing two or three fluids from measured capillary pressure (P_c)–saturation (S) relations. The thermodynamic treatment of two-fluid P_c–S relations presented by Morrow (1970) served as the basis for the predictions. In media containing two fluids (air–oil, air–water, oil–water), the solid–nonwetting interfacial area (A^*_{sN}) equaled zero when the solid was completely wetted by the wetting fluid. The area under the P_c–S curve was directly proportional to the nonwetting–wetting interfacial area (A^*_{NW}). If the solid surface was not completely wetted by one fluid, A^*_{NW} and A^*_{sN} were estimated by weighed partitioning of the area under the P_c–S curve. For porous media with fractional wettability, the procedure was applied separately to water- and oil-wet regions. The values of A^*_{NW} and A^*_{sN} were highest and lowest, respectively, in systems that were strongly wetted. In three-fluid media the wetting and spreading behavior of the liquids greatly affected the estimated interfacial areas. For a water-wet medium with a continuous intermediate oil phase, the interfacial areas were predicted from P_c–S data in a similar manner as for two-fluid media. The oil–water and oil–solid interfacial areas were estimated from the oil–water P_c–S curve, while the air–oil interfacial area was obtained from the air–oil P_c–S curve. For a fractional wettability or oil-wet medium there may be as many as six interfaces. These interfacial areas were estimated from three-fluid P_c–S relations based on previously developed methods for predicting three-fluid P_c–S relations from two-fluid data. © 1997 Elsevier Science B.V.

* Corresponding author. E-mail: fleij@ussl.ars.usda.gov.

0169-7722/97/$17.00 © 1997 Elsevier Science B.V. All rights reserved.
PII S0169-7722(96)00048-4

1. Introduction

The areas of fluid–fluid and fluid–solid interfaces are important parameters for the research and management of flow and transport processes in porous media. The capillary pressure (P_c) and permeability functions depend on interfacial areas (Rapoport and Leas, 1951), although they are typically modeled as functions of fluid saturation (S). Mass transfer processes such as adsorption, dissolution, and volatilization are all proportional to interfacial areas (Pfannkuch, 1984; Miller et al., 1990). Interfacial areas are also important for modeling colloidal and microbial transport (Streile et al., 1991; Wan and Wilson, 1994). Hence, knowledge of the interfacial areas would facilitate the quantification and numerical simulation of a variety of flow and transport processes; including remediation strategies for organic contamination (i.e., vapor extraction, use of surfactants, and bioremediation).

Direct measurement of two-fluid interfacial areas is difficult (Morrow, 1970; Powers et al., 1992). Emerging technologies such as nuclear magnetic resonance imaging, scanning probe microscopy, optical microscopy, and photoluminescent volumetric imaging may facilitate the measurement of interfacial areas (Ronen et al., 1986; Herman and Lemasters, 1993; Wiesendanger, 1994; Montemagno and Gray, 1995). Alternatively, indirect methods for quantifying the interfacial area of two-fluid media include the use of the capillary tube model (Cary, 1994), the ideal soil model (Gvirtzman and Roberts, 1991), interfacial tracers (Saripalli et al., 1995), and a thermodynamic approach (Leverett, 1941; Morrow, 1970).

The capillary tube model uses the experimental P_c–S relation to estimate the pore-size distribution according to the capillary law; the total area of the fluid–fluid interface is then obtained by summing up the hypothetical interfacial areas for all drained capillary tubes at a given P_c. The ideal soil model uses well defined packings of spheres for which the interfacial areas were calculated at a low wetting fluid saturation (Gvirtzman and Roberts, 1991). Both the capillary tube and ideal soil models simplify the solid geometry. Furthermore, the capillary tube model also assumes complete wetting of the solid (Cary, 1994). Interfacial tracers accumulate at interfaces, the mass of accumulated chemical at, for example, an oil–water interface is proportional to the interfacial area. Finally, the thermodynamic approach relates a measured P_c–S curve to the work required for changing the interfacial areas. Both the use of interfacial tracers and the thermodynamic approach are appealing since a description of the solid geometry is not required. Little work has been devoted to estimate interfacial areas for media containing more than two fluids.

The number of interfaces is primarily determined by the interfacial tensions. These determine the contact angle (ϕ) at the solid (s), lighter fluid (l), and denser fluid (d) contact line according to Young's equation:

$$\cos(\phi_{\mathrm{sld}}) = \frac{\sigma_{\mathrm{sl}} - \sigma_{\mathrm{sd}}}{\sigma_{\mathrm{ld}}} \tag{1}$$

where σ is the interfacial tension (N m^{-1}) and the subscripts indicate the phases. Three interfaces (sl, sd, ld) are possible in two-fluid media. If $\phi_{\mathrm{sld}} = 0°$ or 180°, the solid is completely wetted by one fluid and only two interfaces exist (sd or sl, and ld). In case

$\phi_{sld} < 90°$, the denser fluid is the wetting fluid (W) and the lighter fluid is the nonwetting fluid (N). For $\phi_{sld} > 90°$, the roles of the denser and lighter fluids are reversed. In a three-fluid medium the interfacial tensions also determine the coefficient for spreading ($\Sigma_{I/W}$) of an intermediate fluid (I) on a wetting fluid in the presence of a nonwetting fluid:

$$\Sigma_{I/W} = \sigma_{NW} - (\sigma_{NI} + \sigma_{IW}) \tag{2}$$

Six interfaces are possible (viz., sW, sI, sN, IW, NI, NW) for a nonspreading intermediate fluid (i.e., $\Sigma_{I/W} < 0$). On the other hand, only three interfaces (sW, IW, NI) exist for a spreading intermediate fluid (i.e., $\Sigma_{I/W} > 0$) and a solid that is strongly wetted by one fluid.

The objective of this paper is to further develop and apply the approach by Morrow to estimate the interfacial areas in multi-fluid soil systems from measured two- and three-fluid P_c–S relations for a variety of wettabilities. Previous attempts to calculate interfacial areas from P_c–S data have been limited to two-fluid systems, which were assumed to be perfectly wetted ($\phi_{sNW} = 0°$) (Leverett, 1941; Rapoport and Leas, 1951; Morrow, 1970; and Cary, 1994). The experimental two-fluid (air–oil, air–water, oil–water) and three-fluid (air–oil–water) P_c–S data used for this purpose are presented and discussed by Bradford and Leij (1995a,b, 1996).

2. Materials and methods

The porous medium consisted of several blasting sands (Corona Industrial Sand Company, Corona, CA 91718): 12.6% each of ASTM sieve sizes #12 (radius, $R \approx 0.9$ mm) and #16 ($R \approx 0.75$ mm), 25.2% each of #20 ($R \approx 0.45$ mm) and #30 ($R \approx 0.3$ mm), and 8.2% each of #60 ($R \approx 0.125$ mm), #70 ($R \approx 0.1$ mm), and #90 ($R \approx 0.075$ mm). Columns were packed with a predetermined mass of the blasting sand mixture to obtain a dry bulk density (ρ_b) of 1.71 g cm^{-3}. The specific density (ρ_s) of the sand was 2.65 g cm^{-3}. Using these values for ρ_b, ρ_s, and R and assuming that the solid consists of spherical particles, a theoretical solid surface area per unit pore volume (A_s^*) is 233 cm^2 cm^{-3}. A more realistic estimate of $A_s^* = 650$ cm^2 cm^{-3} was obtained using the procedure outlined on p. 570 of Adamson (1990). This estimate of A_s^* likely neglects microporosity. A value of $A_s^* = 5814$ cm^2 cm^{-3} was determined by adsorption of 720 ppm krypton, modeled by the single BET equation (Brunauer et al., 1938), using a Quantasorb Jr. (Quantachrome Corp., Syosset, NY). The surface area determined by adsorption may not be useful for flow problems since it does not correspond to the surface area pertinent to fluid flow (Collins, 1961); the former may be several times greater than the area estimated from geometric calculations or scanning electron microscopy (Anbeek, 1993).

Air (a), water (w), and soltrol 220 (Phillips Petroleum Company, Bartlesville, OK 74004), which is an oil (o) composed of C_{13}–C_{17} hydrocarbons with a fluid density of 0.8 g cm^{-3}, were used as fluids. The average equilibrium surface and interfacial

tensions were measured with a du Noüy ring (du Noüy, 1919) to be $\sigma_{aw} = 0.072$ N m^{-1}, $\sigma_{ao} = 0.024$ N m^{-1}, and $\sigma_{ow} = 0.026$ N m^{-1}; variations between measurements were less than three percent. We measured $\sigma_{aw}^{c} = 0.052$ N m^{-1} as the interfacial tension of the soltrol contaminated air–water interface. The value of σ_{aw}^{c} is physically more realistic than σ_{aw} since even a trace amount of oil can greatly affect σ_{aw} (Corey, 1986). The coefficients of spreading calculated according to (2), using $\sigma_{aw} = 0.072$ N m^{-1}, were $\Sigma_{o/w} = 0.022$ N m^{-1} and $\Sigma_{w/o} = -0.074$ N m^{-1}. Similarly, the contaminated coefficients of spreading, calculated with $\sigma_{aw}^{c} = 0.052$ N m^{-1}, were $\Sigma_{o/w}^{c} = 0.002$ N m^{-1} and $\Sigma_{w/o}^{c} = -0.054$ N m^{-1}.

Blasting sands were treated with the organosilane compounds vinyltriethoxysilane (VTS) or octadecyltrichlorosilane (OTS) to obtain media with different degrees of wettability (Anderson et al., 1991). The untreated sands were strongly water-wet, while the VTS and, especially, the OTS treated sands were oil-wet in oil–water systems. Media with fractional wettability were obtained by mixing untreated and OTS treated blasting sands.

The wettability of the porous medium was quantified by fitting an effective macroscopic contact angle, ϕ_{sld}, to measured P_c–S data and interfacial tensions. Scaling P_c–S data for a particular medium suggests that if $\phi_{sao} = 0°$, ϕ_{slw} (where l denotes a or o) may be determined as (Bradford and Leij, 1995a):

$$\cos(\phi_{slw}) = \frac{\sigma_{ao} P_{lw}(\bar{S}_w^{lw})}{\sigma_{lw} P_{ao}(\bar{S}_o^{ao})} \tag{3}$$

where $P_{lw} = P_l - P_w$ and $P_{ao} = P_a - P_o$ are capillary pressures, and $\bar{S}_w^{lw} = (S_w^{lw} - S_{rw}^{lw})/(1 - S_{rw}^{lw} - S_{rl}^{lw})$ and $\bar{S}_o^{ao} = (S_o^{ao} - S_{ro}^{ao})/(1 - S_{ro}^{ao} - S_{ra}^{ao})$ are the effective water and oil saturations, respectively, with the subscript r denoting a residual saturation. We adopt the convention that the subscript of the saturation S or $\bar{S}$, which is expressed as volume of fluid per unit volume of pore space, indicates the fluid to which the saturation pertains and the superscripts denote all fluids present in the medium. The receding (ϕ_{sow}^{R}) and advancing (ϕ_{sow}^{A}) contact angles were obtained by fitting (3) to drainage and imbibition P_c–S data, respectively. Note that (3) assumes that the pores in the medium may be viewed as capillary tubes. Melrose (1965) reported that the ideal soil model predicted strikingly different effects of wettability on the imbibition curve due to pore geometry effects. In contrast, Morrow (1976) measured P_c–S curves for a variety of media and wettabilities, and found only a "minor effect" of pore geometry on the apparent contact angles (cf. Eq. (3)) from one medium to another.

3. Two-fluid interfacial areas

3.1. Thermodynamic description of capillary pressure

Fig. 1 shows a schematic of a hypothetical P_c–S measurement system consisting of a porous medium containing two fluids (oil and water) in contact with their respective

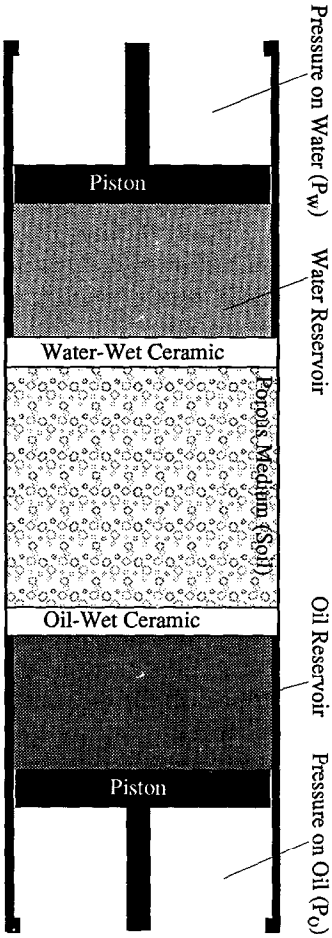

Fig. 1. Schematic of two-fluid system for which the thermodynamic description of capillarity is developed.

fluid reservoirs. The fluid saturations are changed by doing external work (W_{ext}) on the system through the pistons according to:

$$\delta W_{ext} = P_N \varepsilon V_b \, \delta S_N^{NW} + P_W \varepsilon V_b \, \delta S_W^{NW} = -P_{NW} \varepsilon V_b \, \delta S_W^{NW} \tag{4}$$

where δ denotes an infinitesimal change, ε is the porosity, V_b is the bulk volume of the porous medium, P_{NW} is the capillary pressure ($P_c = P_{NW} = P_N - P_W$), and $\delta S_W^{NW} = -\delta S_N^{NW}$. The force acting on the frictionless piston gives the fluid pressure, usually with respect to atmospheric pressure. The capillary pressure, P_c, follows directly from the difference in pressure of the pistons in contact with the nonwetting and wetting reservoirs.

Two-fluid media contain three bulk phases (solid, wetting fluid, and nonwetting fluid) with three possible interfaces (solid–wetting, solid–nonwetting, and nonwetting–wet-

ting). For the closed system (constant mass) shown in Fig. 1 the first law of thermodynamics states that the change in the total energy of the system, $\mathrm{d}E$, is equal to

$$\mathrm{d}E = \delta q + \delta W_{i+p} = T\,\mathrm{d}\Lambda + \sum_{i=1}^{N_i} \sigma_i\,\delta A_i - \sum_{p=1}^{N_p} P_p\,\delta V_p \tag{5}$$

where N_i and N_p are the number of interfaces (i = sN, sW, or NW) and bulk phases (p = s, W, or N). The value of δq, the heat flowing into the system, equals the product of the temperature (T) and the change in entropy (Λ) of the system. The value of δW_{i+p} is equal to the reversible work done on the interfaces ($\Sigma\sigma_i\delta A_i$) and bulk phases ($\Sigma P_p\delta V_p$). Note that σ_i and A_i are the interfacial tension and interfacial area, and P_p and V_p are the pressure and volume of the bulk phase. Reversible work ($\Sigma\sigma_i\delta A_i$) is required to change the interfacial areas since the net force acting on molecules is different at the interface than in the bulk phase (Gibbs, 1961). Similarly, reversible work ($\Sigma P_p\delta V_p$) is also required to compress or expand a phase.

The change in Helmholtz free energy, $\mathrm{d}F$, of the above system is equal to

$$\mathrm{d}F = \mathrm{d}E - \mathrm{d}(T\Lambda) = -\Lambda\,\mathrm{d}T + \sum_{i=1}^{N_i} \sigma_i\,\delta A_i - \sum_{p=1}^{N_p} P_p\,\delta V_p \tag{6}$$

For an isothermal system ($\mathrm{d}T = 0$) with incompressible phases ($\delta V_p = 0$), $\mathrm{d}F$ is equal to $\Sigma\sigma_i\delta A_i$. By similar reasoning, $\mathrm{d}F$ for the surroundings is equal to the change in external work δW_{ext} (cf. Eq. (4)). At equilibrium the change in Helmholtz free energy of the system and surroundings is zero, hence:

$$-P_{\mathrm{NW}}\,\varepsilon V_{\mathrm{b}}\,\delta S_{\mathrm{W}}^{\mathrm{NW}} = \sum_{i=1}^{N_i} \sigma_i\,\delta A_i \tag{7}$$

The total solid surface area, A_{s}, is constant and $\delta A_{\mathrm{sW}} = -\delta A_{\mathrm{sN}}$. We assume that Young's equation, which follows from a momentum balance for a contact line at the micro-scale (cf. Hassanizadeh and Gray, 1993), may also be applied to macroscopic systems such as the one given schematically in Fig. 1. In this case Eq. (7) can be written as

$$-P_{\mathrm{NW}}\,\varepsilon V_{\mathrm{b}}\,\delta S_{\mathrm{W}}^{\mathrm{NW}} = \sigma_{\mathrm{NW}}\cos(\phi_{\mathrm{sNW}})\delta A_{\mathrm{sN}} + \sigma_{\mathrm{NW}}\,\delta A_{\mathrm{NW}} \tag{8}$$

We can rewrite (8) by expressing the interfacial areas per unit pore volume ($A_i^* = A_i/\varepsilon V_{\mathrm{b}}$) as

$$-P_{\mathrm{NW}}\,\delta S_{\mathrm{W}}^{\mathrm{NW}} = \sigma_{\mathrm{NW}}\cos(\phi_{\mathrm{sNW}})\delta A_{\mathrm{sN}}^* + \sigma_{\mathrm{NW}}\,\delta A_{\mathrm{NW}}^* \tag{9}$$

Morrow (1970) justifies the use of (9) to describe hysteretic P_{c}–S relations since: (i) P_{c}–S data exhibit permanent hysteresis (i.e., the difference between imbibition and drainage curves cannot be reduced by allowing more time for measurement of P_{c}–S data points); and (ii) both drainage and imbibition processes consist of a series of reversible displacements and spontaneous redistributions (haines jumps). The heat of wetting associated with imbibition is minuscule in comparison to the heat capacity of the system, and was, therefore, assumed to have negligible effects on the calculated interfacial areas

(Morrow, 1970). Hence, (9) relates an observable capillary pressure, P_{NW}, to changes in interfacial areas A^*_{sN} and A^*_{NW} as a result of changes in saturation. External work is required during drainage of the wetting fluid to increase the interfacial areas (A^*_{sN} and A^*_{NW}). In contrast, the system works on the surroundings during imbibition of the wetting fluid to decrease A^*_{sN} and A^*_{NW}.

After dividing (9) by δS_W^{NW} and integrating with respect to S_W^{NW} and assuming that σ_{NW} and ϕ_{sNW} are constant, we obtain (cf. Eq. (68) of Morrow (1970)):

$$\Phi_{NW}(S_W^{NW}) = -\int_{\chi}^{S_W^{NW}} P_{NW}(z)\,dz = \sigma_{NW}\cos(\phi_{sNW})\int_{\chi}^{S_W^{NW}} \frac{\delta A^*_{sN}}{\delta z}\,dz + \sigma_{NW}\int_{\chi}^{S_W^{NW}} \frac{\delta A^*_{NW}}{\delta z}\,dz \tag{10}$$

where the limit of integration χ is equal to the value of S_W^{NW} when $P_{NW} = 0$, and z is a dummy variable. For the primary (Morrow, 1970) or initial (Klute, 1986) drainage curve the medium is initially saturated with the wetting fluid and $\chi = 1$. For the main imbibition and drainage curves, following the terminology of Klute (1986), we have $\chi = 1 - S_{rN}^{NW}$, where S_{rN}^{NW} is the residual nonwetting saturation. According to (10) the area under the P_{NW}–S_W^{NW} curve, $\Phi_{NW}(S_W^{NW})$, is related to $A^*_{sN}(S_W^{NW})$ and $A^*_{NW}(S_W^{NW})$ by:

$$\Phi_{NW}(S_W^{NW}) + C_{NW} = \sigma_{NW}\cos(\phi_{sNW})\,A^*_{sN}(S_W^{NW}) + \sigma_{NW}\,A^*_{NW}(S_W^{NW}) \tag{11}$$

where C_{NW} is a constant of integration equal to $\sigma_{NW}A^*_{NW}(\chi)$. Note that during primary drainage $A^*_{sN}(\chi) = A^*_{NW}(\chi) = 0$ since only the wetting fluid is present. Similarly, during subsequent imbibition and drainage cycles $A^*_{sN}(\chi) \approx 0$; the nonwetting fluid is entrapped in the center of pores (Chatzis et al., 1983). Furthermore $\Phi_{NW}(\chi) = 0$ since, by definition, $P_{NW}(\chi) = 0$. The relative contributions of C_{NW} and Φ_{NW} to the determination of the interfacial areas depend on the saturation. If $S_W^{NW} = 1 - S_{rN}^{NW}$ the value of C_{NW} dominates, while for $S_W^{NW} = S_{rW}^{NW}$ the value of Φ_{NW} dominates. At the latter saturation it may be desirable to independently determine a constraint for Φ_{NW}.

Measured P_{NW}–S_W^{NW} data were used to estimate values of $\Phi_{NW}(S_W^{NW})$ and C_{NW}. The P_{NW}–S_W^{NW} data were first described by (Bradford and Leij, 1995b):

$$P_c(S_W^{NW}) = \frac{1}{\alpha}\left[(S_W^{NW})^{n/(1-n)} - 1\right]^{1/n} - \lambda \tag{12}$$

Table 1 lists the parameters (n, α, λ) obtained by fitting this modified model of van Genuchten (1980) to the P_c–S data, as well as, the regression coefficient (r^2) for the goodness of fit. The values of S_{rW} (S_{rW}^{NW} or S_{rW}^{NIW}) and S_{rN} (S_{rN}^{NW} or S_{rN}^{NIW}) are also shown in Table 1; S_{rW} and S_{rN} correspond to the lowest values of S_W^{NW} or S_W^{NIW} and S_N^{NW} or S_N^{NIW} that were attained during the experiment. A value of $\Phi_{NW}(S_W^{NW})$ was then obtained by numerically integrating the P_c–S model (cf. Eq. (12)) according to (10).

The value of C_{NW} was determined by assuming that the nonwetting fluid was entrapped as spheres with a saturation-dependent radius, $R(S_W^{NW})$. The radii ranged in value from $R(1)$ to $R(1 - S_{rN}^{NW})$. The P_{NW}–S_W^{NW} curve in the range $1 - S_{rN}^{NW} < S_W^{NW} < 1$ was arbitrarily divided into four regions with increment $\Delta S_W^{NW} = S_{rN}^{NW}/4$ and radius

Table 1
Measured (S_{rN} and S_{rW}) and fitted (n, α, and λ) values obtained from $P_c - S$ data according to (12), as well as, the coefficient of regression for the goodness of fit (r^2)

Figure	Path	$P_c - S$	S_{rW}	S_{rN}	λ (cm)	α (cm^{-1})	n	r^2
Fig. 3	D	$P_{ao} - S_o^{ao}$	0.12	0.00	0.00	0.078	4.415	0.967
	I	$P_{ao} - S_o^{ao}$	0.12	0.13	11.4	0.052	4.415	0.967
Fig. 4a, Fig. 4b [a]	D	$P_{aw} - S_w^{aw}$	0.20	0.00	0.00	0.035	3.248	0.989
	I	$P_{aw} - S_w^{aw}$	0.20	0.43	0.00	0.065	2.419	0.929
Fig. 4a, Fig. 4b [b]	D	$P_{aw} - S_w^{aw}$	0.26	0.00	0.00	0.041	4.754	0.977
	I	$P_{aw} - S_w^{aw}$	0.26	0.03	0.00	0.083	2.642	0.848
Fig. 6	D	$P_{ow} - S_w^{ow}$	0.22	0.13	7.64	0.100	2.891	0.943
	I	$P_{ow} - S_w^{ow}$	0.22	0.13	7.64	0.610	1.534	0.934
Fig. 8a, Fig. 8b	D	$P_{ao} - S_{tl}^{aow}$	0.28	0.13	0.00	0.837	3.893	0.944
	I	$P_{ao} - S_{tl}^{aow}$	0.28	0.13	0.00	0.122	2.779	0.932
	D	$P_{ow} - S_w^{aow}$	0.14	0.13	151.	0.006	15.85	0.990
	I	$P_{ow} - S_w^{aow}$	0.14	0.13	0.00	0.963	1.500	0.898
Fig. 9a	D	$P_{ow} - S_w^{aow}$	0.25	0.11	10.8	0.213	1.813	0.823
	I	$P_{ow} - S_w^{aow}$	0.25	0.11	10.8	2.269	1.387	0.792
Fig. 9b	D	$P_{ao} - S_{tl(o)}^{aow}$	0.40	0.12	0.00	0.077	3.958	0.922
	I	$P_{ao} - S_{tl(o)}^{aow}$	0.40	0.12	0.00	0.100	3.650	0.827
Fig. 9c	D	$P_{aw} - S_{tl(w)}^{aow}$	0.40	0.06	0.00	0.076	2.048	0.894
	I	$P_{aw} - S_{tl(w)}^{aow}$	0.40	0.06	0.00	0.547	1.373	0.901

D: drainage.
I: imbibition.
[a] untreated.
[b] VTS.

$R_j(S_{jW}^{NW})$; where $S_{jW}^{NW} = 1 - S_{rN}^{NW} + (2j-1)\Delta S_W^{NW}/2$ and $j = 1,2,3,4$. The surface area per unit pore volume for each pore class was determined as the product of the surface area of the sphere ($4\pi R_j^2$) and the number of spheres per unit pore volume, $\Delta S_W^{NW}/(4\pi R_j^3/3)$. Addition of the surface areas of the four pore classes yields:

$$C_{NW} = 3\sum_{j=1}^{4} \frac{\sigma_{NW}\,\Delta S_W^{NW}}{R_j\left(S_{jW}^{NW}\right)} \quad \left(1 - S_{rN}^{NW} < S_{jW}^{NW} < 1\right) \tag{13}$$

Values for $R_j(S_{jW}^{NW})$ were estimated from the corresponding $P_{NW}(S_{jW}^{NW})$ values of the primary drainage P_{NW}–S_W^{NW} curve according to the capillary law as:

$$C_{NW} = \frac{3}{2}\sum_{j=1}^{4} \frac{P_{NW}\left(S_{jW}^{NW}\right)\Delta S_W^{NW}}{\cos(\phi_{sNW})} \quad \left(1 - S_{rN}^{NW} < S_{jW}^{NW} < 1\right) \tag{14}$$

Recall that $C_{NW} = 0$ for primary drainage, while for main drainage and imbibition $C_{NW} > 0$ provided that $S_{rN}^{NW} > 0$.

Estimates for the interfacial areas can now be obtained by substituting values for $\Phi_{NW}(S_W^{NW})$ (cf. Eq. (10)) and C_{NW} (cf. Eq. (14)) into Eq. (11). Fig. 2 shows a generic P_c–S curve with associated parameters $\Phi_{NW}(S_W^{NW})$ and C_{NW}. Note that $\Phi_{NW}(S_W^{NW})$ is the area under the P_c–S curve and C_{NW} is a constant of integration due to entrapment of nonwetting fluid in the region $1 - S_{rN}^{NW} < S_W^{NW} < 1$. The value of A_{NW}^* is assumed to

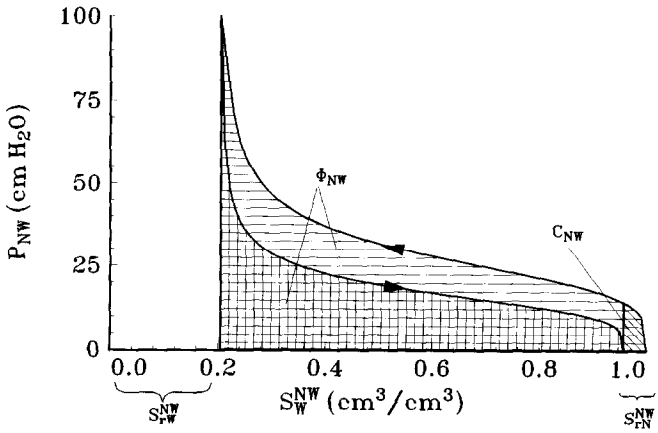

Fig. 2. Generic P_c-S curve with associated parameters $\Phi_{NW}(S_W^{NW})$ and C_{NW}.

reach its maximum when $S_W^{NW} = S_{rW}^{NW}$. Payne (1953) also found that during drainage of the wetting fluid A_{NW}^* approaches A_s^* as S_W^{NW} approaches S_{rW}^{NW}. For low S_W^{NW} (i.e., $S_W^{NW} < S_{rW}^{NW}$), $\Phi_{NW}(S_W^{NW})$ cannot be quantified due to the lack of reliable P_c–S data. Since the contribution to $\Phi_{NW}(S_W^{NW})$ of the area for which $S_W^{NW} < S_{rW}^{NW}$ is likely substantial, we can not reliably estimate areas in this saturation domain. We emphasize that this method is most suitable for estimating changes in interfacial areas (cf. Morrow, 1970) and an evaluation of the procedure based on independent estimates of the solid surface or area of pore space is not possible. Gvirtzman and Roberts (1991) found that for $S_W^{NW} < S_{rW}^{NW}$, according to the ideal soil model, a decrease in S_W^{NW} leads to a reduction in A_{NW}^* because of discontinuity of the wetting phase. Obviously, $A_{NW}^* = 0$ if $S_W^{NW} = 0$ and $S_W^{NW} = 1$, $A_{sN}^* = 0$ if $S_W^{NW} = 1$, and $A_{sN}^* = A_s^*$ if $S_W^{NW} = 0$.

3.2. Zero contact angle

For the simple case of complete wetting of the solid by one fluid $A_{sN}^*(S_W^{NW}) = 0$, (11) reduces to (Leverett, 1941):

$$A_{NW}^*(S_W^{NW}) = \frac{\Phi_{NW}(S_W^{NW}) + C_{NW}}{\sigma_{NW}} \tag{15}$$

Bradford and Leij (1995a) observed complete wetting of the solid by the oil for an air–oil system due to the low value for σ_{ao} of 0.024 N m^{-1}. Fig. 3 shows the air–oil interfacial area, $A_{ao}^*(S_o^{ao})$, as calculated from the primary drainage and main imbibition cycles of the P_{ao}–S_o^{ao} curve. The value of A_{ao}^* is generally larger during drainage than during imbibition because of hysteresis in the P_c–S curve. The value of A_{ao}^* for $S_o^{ao} = 1 - S_{ra}^{ao} = 0.87$ is slightly larger during main imbibition than during primary drainage ($S_{ra}^{ao} = 0$) due to air entrapment. The maximum estimate for A_{ao}^*, occurring during drainage at $S_o^{ao} = 0.13$, is 74% the estimate for $A_s^* = 650$ cm^2 cm^{-3}.

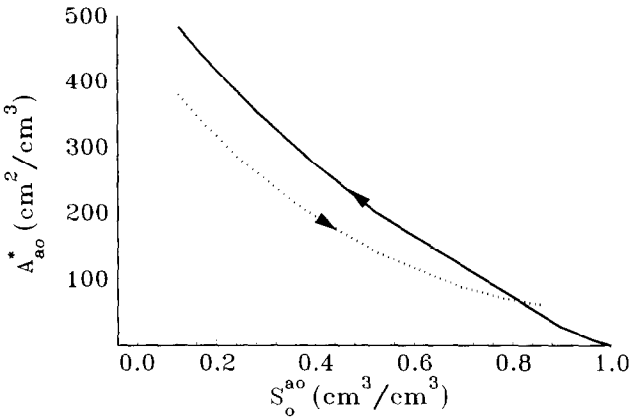

Fig. 3. The calculated $A^*_{ao}(S^{ao}_o)$ relations during primary drainage and main imbibition.

Leverett (1941) and Rapoport and Leas (1951) previously applied variations of the thermodynamic approach (cf. Eq. (15)) to estimate $A^*_{NW}(S^{NW}_W)$ for systems having perfect wettability. The capillary tube model has also been employed to evaluate $A^*_{NW}(S^{NW}_W)$ (Cary, 1994) for such systems. According to this model $A^*_{NW}(S^{NW}_W)$ is related to the pore-size distribution and, hence, the P_c–S relation as:

$$A^*_{NW}(S^{NW}_W) = -2\int_1^{S^{NW}_W} \frac{dz}{R(z)} = -\int_1^{S^{NW}_W} \frac{P_{NW}(z)}{\sigma_{NW}} dz = \frac{\Phi(S^{NW}_W)}{\sigma_{NW}} \tag{16}$$

Note that (15) and (16) are identical during primary drainage, but differ during main drainage and imbibition because (16) neglects interfacial area associated with entrapped nonwetting fluid (C_{NW}). Gvirtzman and Roberts (1991) used the ideal soil model to predict the interfacial areas in the region $S^{NW}_W < S^{NW}_{rW}$, whereas the thermodynamic approach is only applicable in the region $S^{NW}_W > S^{NW}_{rW}$. Consequently, a quantitative comparison between these two techniques is not possible.

3.3. Nonzero contact angle

If the solid of the porous medium is not completely wetted by the wetting fluid ($\phi_{sNW} > 0$), a solid–nonwetting fluid interface occurs with area A^*_{sN}. In this case we propose to determine $A^*_{sN}(S^{NW}_W)$ and $A^*_{NW}(S^{NW}_W)$ from the P_{NW}–S^{NW}_W curve and C_{NW} (Eq. (11)) according to

$$A^*_{sN}(S^{NW}_W) = f(\phi_{sNW}) \frac{\Phi_{NW}(S^{NW}_W) + C_{NW}}{\sigma_{NW}\cos(\phi_{sNW})} \tag{17}$$

$$A^*_{NW}(S^{NW}_W) = [1 - f(\phi_{sNW})] \frac{\Phi_{NW}(S^{NW}_W) + C_{NW}}{\sigma_{NW}} \tag{18}$$

where $f(\phi_{sNW})$ is an empirical weighing function for which we used

$$f(\phi_{sNW}) = \tfrac{1}{2}[1 - \cos(\phi_{sNW})] \tag{19}$$

In (17), (18), and (19) the denser fluid is the wetting fluid ($\phi_{sNW} = \phi_{sld}$) for $\phi_{sld} < 90°$ and the nonwetting fluid ($\phi_{sNW} = 180° - \phi_{sld}$) for $90° \leq \phi_{sld} < 180°$. For a given saturation $f(\phi_{sNW})$ is equivalent to half the difference between Φ_{NW} for $\phi_{sNW} = 0°$ and $\phi_{sNW} > 0°$, with respect to Φ_{NW} for $\phi_{sNW} = 0°$. Results by Morrow (1976) support the hypothesis (inherent to Eq. (19)) that at a given saturation A^*_{NW} decreases (i.e., P_{NW} decreases) and A^*_{sN} increases (i.e., S^{NW}_{rW} increases) for greater ϕ_{sNW}. The value of ϕ_{sld} is hence an important parameter for quantifying $A^*_{NW}(S^{NW}_W)$ and $A^*_{sN}(S^{NW}_W)$.

Bradford and Leij (1995a) measured P_{aw}–S^{aw}_w curves for media with the same pore-size distribution but with different hydrophobicity. The respective values of ϕ^R_{saw} and ϕ^A_{saw} were 0° and 32.7° for the untreated (hydrophilic) medium and 35.6° and 52.2°

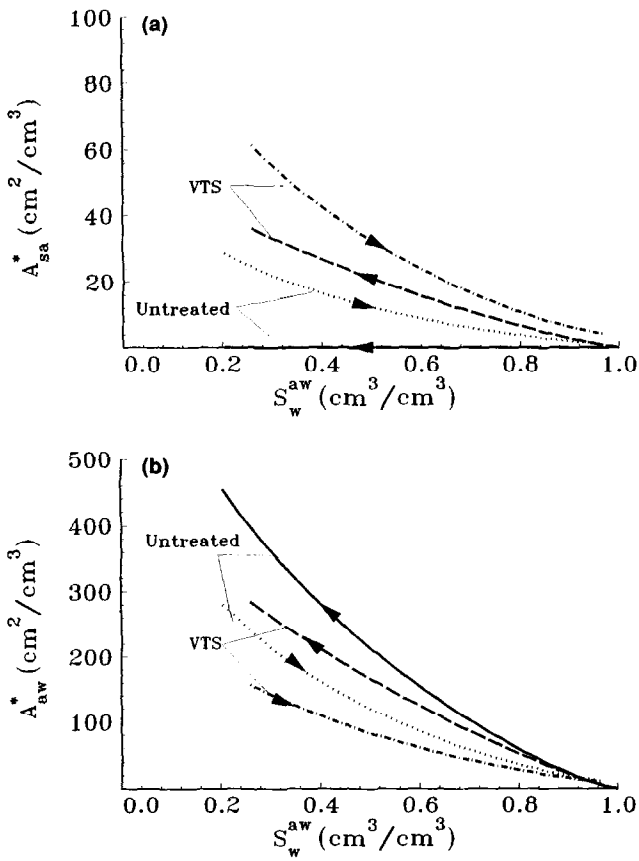

Fig. 4. The calculated (a) $A^*_{sa}(S^{aw}_w)$ and (b) $A^*_{aw}(S^{aw}_w)$ relations during primary drainage and main imbibition for the untreated and VTS media. The respective values of ϕ^R_{saw} and ϕ^A_{saw} were 0° and 32.7° for the untreated medium and 35.6° and 52.2° for the VTS medium.

for the VTS (hydrophobic) medium. Fig. 4a and Fig. 4b show the corresponding $A^*_{sa}(S^{aw}_w)$ and $A^*_{aw}(S^{aw}_w)$ relations, calculated with (17) and (18), respectively, during primary drainage and main imbibition. As the medium becomes more hydrophobic, A^*_{sa} increases and A^*_{aw} decreases at a given S^{aw}_w (cf. Fig. 3). The estimated value of A^*_{aw} is larger for drainage than for imbibition due to hysteresis. Although P_{aw} is larger than P_{ao} for a given saturation, A_{aw} and A_{ao} are of a similar magnitude since the area under the P_c–S curve is divided by the corresponding interfacial tension; $(\Phi_{ao} + C_{ao})/\sigma_{ao}$ (cf. Eq. (15)) and $(\Phi_{aw} + C_{aw})/\sigma^*_{aw}$ (cf. Eq. (18)).

3.4. Fractional wettability

The wettability of many natural porous media may be highly variable and position dependent (Brown and Fatt, 1956). This so-called "fractional wettability" is not apparent in air–oil and air–water systems since air is usually the nonwetting fluid ($P_c = P_a - P_w > 0$). In fractional wettability media containing oil and water we define the capillary pressure as $P_{ow} = P_o - P_w$ with respect to water as the "reference" wetting fluid. Fig. 5 shows the main imbibition and drainage curves of the P_{ow}–S^{ow}_w relation obtained for a medium that consists of 25% untreated and 75% OTS treated sands. Note that both positive and negative values of P_{ow} occur due to the presence of water- and oil-wet solids. The segments labeled 1 and 4 correspond to the imbibition and drainage of water from "water-wet" sites, respectively, while the segments labeled 2 and 3 indicate drainage and imbibition of oil from the "oil-wet" sites. We will therefore apply the previously discussed techniques for estimating the interfacial areas separately to the water- and oil-wet branches of the P_{ow}–S^{ow}_w relation. The water saturation corresponding to $P_{ow} = 0$ is denoted in Fig. 5 by χ_{MD} for main drainage and χ_{MI} for main imbibition.

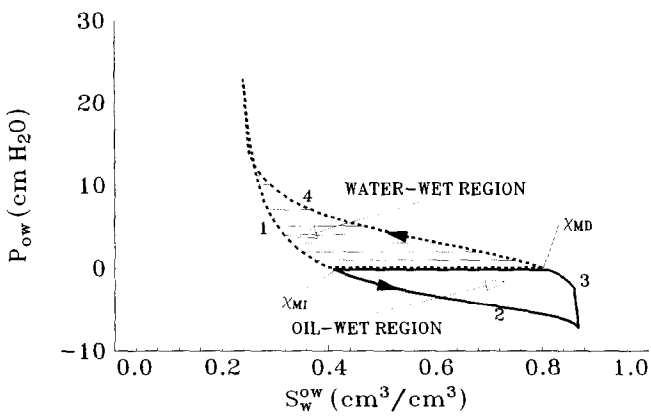

Fig. 5. The P_{ow}–S^{ow}_w relation for the 75% OTS medium with segments 1 and 4 corresponding to the imbibition and drainage of water from water-wet sites, respectively, and 2 and 3 for the drainage and imbibition of oil from the oil-wet sites, respectively. The saturation at which $P_{ow} = 0$ is given by χ_{MD} (main drainage) and χ_{MI} (main imbibition).

We assume that $\phi_{sow} = 0°$ and $A^*_{so}(S^{ow}_w) = 0$ for water-wet solids ($P_{ow} > 0$), and $\phi_{sow} = 180°$ and $A^*_{sw}(S^{ow}_w) = 0$ for oil-wet solids ($P_{ow} < 0$). Eq. (15) is then rewritten for the water-wet region as:

$$A^*_{ow}(S^{ow}_w) = \frac{1}{\sigma_{ow}}[\Phi_{ow}(S^{ow}_w) + C_o] \quad P_{ow} > 0; \chi > S^{ow}_w \tag{20}$$

and for the oil-wet region as:

$$A^*_{ow}(S^{ow}_w) = \frac{1}{\sigma_{ow}}[\Phi_{ow}(S^{ow}_w) + C_w] \quad P_{ow} < 0; \chi < S^{ow}_w \tag{21}$$

Integration of the P_{ow}–S^{ow}_w curve (cf. Eq. (10)) starts at $\chi = \chi_{MD}$ for drainage (segments 3 and 4) and $\chi = \chi_{MI}$ for imbibition (segments 1 and 2). The area under the P_{ow}–S^{ow}_w curve, $\Phi_{ow}(S^{ow}_w)$, is positive for both water- and oil-wet regions according to (20) and (21). The volume of entrapped nonwetting fluid can not be obtained from the measured P_{ow}–S^{ow}_w curve since it is due to oil entrapment for segments 1 and 4 (denoted as C_o), and due to water entrapment for segments 2 and 3 (denoted as C_w). An estimate of A^*_{ow} resulting from entrapped oil, C_o, may be obtained from scaling the constant of integration of an air–oil system C_{ao} by $\sigma_{ow}(1 - F_o)/\sigma_{ao}$; where F_o is the mass fraction of oil-wet solids. Similarly, an estimate of the interfacial area due to entrapped water, C_w, is obtained when C_{ao} is multiplied by $\sigma_{ow}F_o/\sigma_{ao}$. Bradford and Leij (1995b) discussed a method for determining F_o for a fractional wettability medium.

Fig. 6 shows the calculated $A^*_{ow}(S^{ow}_w)$ relationship for the main imbibition and drainage curves of water in a 75% OTS medium (i.e., $F_o = 0.75$). Note that the predicted interfacial area, A^*_{ow}, reaches a minimum at $S^{ow}_w = 0.43$ during imbibition and at $S^{ow}_w = 0.78$ during drainage when $P_{ow} = 0$. An absolute minimum, $A^*_{ow} = 0$, would happen when there is only one liquid (S^{ow}_o or $S^{ow}_w = 0$). The "bumps", occurring at $S^{ow}_w = 0.43$ and $S^{ow}_w = 0.78$, are a consequence of our method of using $C_o = C_{ao}\sigma_{ow}(1 -$

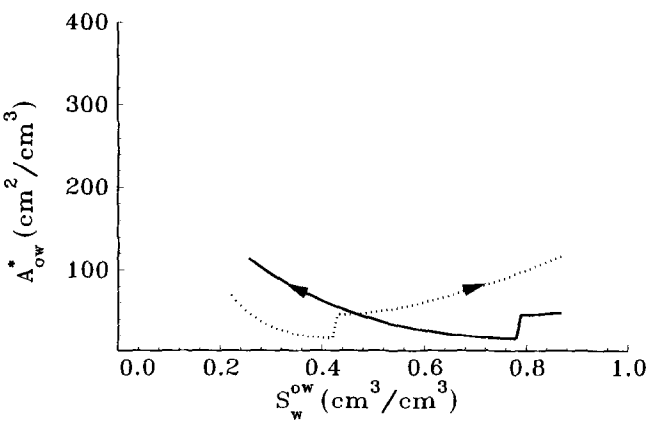

Fig. 6. The $A^*_{ow}(S^{ow}_w)$ relation calculated according to (20) and (21) for the 75% OTS medium during main imbibition and drainage.

$F_o)/\sigma_{ao}$ for branches 1 and 4 and $C_w = C_{ao}\sigma_{ow}F_o/\sigma_{ao}$ for branches 2 and 3. For $S_w^{ow} > 0.46$, the interfacial area is greater for imbibition than drainage of water from oil-wet sites. In this hydrophobic region more energy is required to imbibe water (i.e., drain oil) than to drain water (i.e, imbibe oil). Conversely, it is more difficult if $S_w^{ow} < 0.46$ to drain than to imbibe water from water-wet sites. A comparison of the fluid–fluid areas given in Fig. 6 with those in Fig. 3 and Fig. 4b shows that the 75% OTS oil–water system has significantly lower A_{NW}^*, since there are both water- and oil-wet sites, than the media with uniform wettability.

4. Three-fluid interfacial areas

4.1. Continuous intermediate fluid

The previously discussed approaches for quantifying interfacial areas from P_c–S data of two-fluid systems can also be adapted for three-fluid media. Fig. 7 illustrates a hypothetical system consisting of a porous medium containing three fluids (air, water, and oil) in contact with their respective fluid reservoirs. When the intermediate fluid is continuous, the system contains four bulk phases ($N_p = 4$) and four interfaces ($N_i = 4$). The external work, W_{ext}, done on pistons in contact with the fluid reservoirs to change saturations is given as:

$$\delta W_{ext} = P_N \varepsilon V_b\, \delta S_N^{NIW} + P_I \varepsilon V_b\, \delta S_I^{NIW} + P_W \varepsilon V_b\, \delta S_W^{NIW} \tag{22}$$

In analogy to (9), the external work per unit pore volume done on an isothermal system where the medium and fluids are incompressible, is given by the equilibrium expression:

$$P_N\, \delta S_N^{NIW} + P_I\, \delta S_I^{NIW} + P_W\, \delta S_W^{NIW} = \sigma_{IW}\cos(\phi_{sIW})\delta A_{sI}^* + \sigma_{IW}\, \delta A_{IW}^* + \sigma_{NI} A_{NI}^* \tag{23}$$

Two capillary pressures, P_{IW} and P_{NI}, exist for a continuous intermediate (I) fluid. These pressures are unique functions of S_W^{NIW} and S_{tl}^{NIW}, respectively (Lenhard and Parker, 1988; Ferrand et al., 1990; Bradford and Leij, 1995a). Note that the total liquid saturation, S_{tl}^{NIW}, is defined as $S_W^{NIW} + S_I^{NIW}$. In contrast to A_{NI}^*, the values of A_{sI}^* and A_{IW}^* are influenced by changes in S_W^{NIW} at constant S_{tl}^{NIW} (i.e., $\delta S_N^{NIW} = 0$ and $\delta S_W^{NIW} = -\delta S_I^{NIW}$) since P_{IW} is a function of S_W^{NIW}. The external work associated with changing the area between intermediate and wetting fluids can be written as (cf. Eq. (23)):

$$-P_{IW}\, \delta S_W^{NIW} = \sigma_{IW}\cos(\phi_{sIW})\delta A_{sI}^* + \sigma_{IW}\, \delta A_{IW}^* \tag{24}$$

If we consider changing S_I^{NIW} at a constant S_W^{NIW} ($\delta S_W^{NIW} = 0$ and $\delta S_I^{NIW} = -\delta S_N^{NIW}$), the external work associated with the nonwetting–intermediate fluids interface is given by (cf. Eq. (23))

$$-P_{NI}\, \delta S_I^{NIW} = \sigma_{NI}\, \delta A_{NI}^* \tag{25}$$

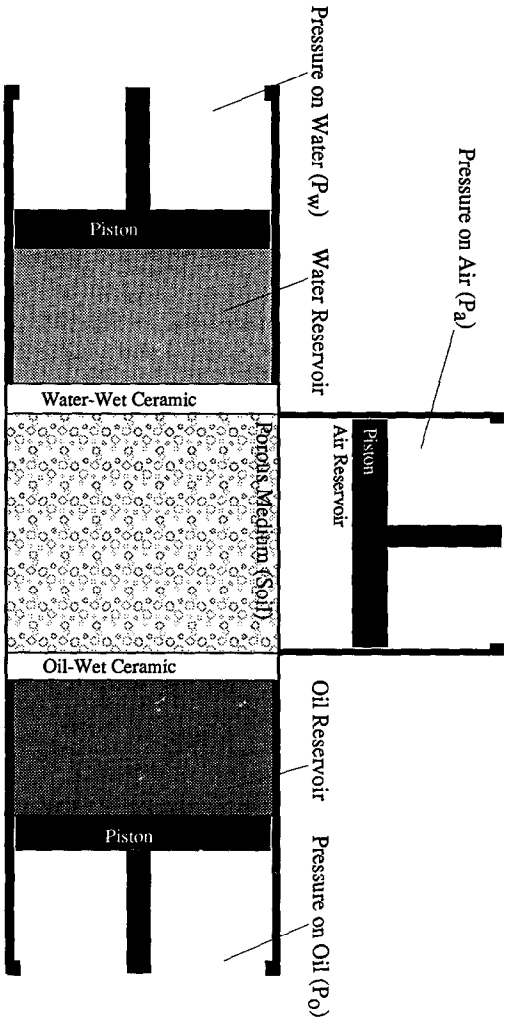

Fig. 7. Schematic of three-fluid system for which the thermodynamic description of capillarity is developed.

If we change S_W^{NIW} at a constant S_I^{NIW} ($\delta S_I^{NIW} = 0$ and $\delta S_W^{NIW} = -\delta S_N^{NIW}$), the external work for changing the interfaces between the nonwetting–intermediate and intermediate–wetting fluids is

$$-P_{NW}\,\delta S_W^{NIW} = -(P_{NI} + P_{IW})\delta S_W^{NIW} = \sigma_{IW}\cos(\phi_{sIW})\delta A_{sI}^* + \sigma_{IW}\,\delta A_{IW}^* + \sigma_{NI}\,\delta A_{NI}^* \tag{26}$$

We have invoked the experimental constraint $P_{NW} = P_{NI} + P_{IW}$. The dependency of P_{IW} on A_{sI} and A_{IW}, according to (24), suggests that P_{NI} mainly depends on A_{NI}^* for changes in S_W^{NIW}. Hence, we write A_{NI}^* as a function of the total liquid saturation, S_{tl}^{NIW}:

$$-P_{NI}\,\delta S_{tl}^{NIW} = \sigma_{NI}\,\delta A_{NI}^* \tag{27}$$

The analogy between (9) and (24) or (27) suggests a similar dependency of the two- and three-fluid interfacial areas on fluid saturations. This reasoning provides the justification for predicting three-fluid from two-fluid P_c–S relations (Leverett's assumption).

Integration of the P_{IW}–S_W^{NIW} curve according to (24) yields:

$$\Phi_{IW}(S_W^{NIW}) + C_{IW} = \sigma_{IW}\cos(\phi_{sIW})\,A_{sI}^*(S_W^{NIW}) + \sigma_{IW}\,A_{IW}^*(S_W^{NIW}) \tag{28}$$

while integration of the P_{NI}–S_{tl}^{NIW} curve according to (27) gives

$$\Phi_{NI}(S_{tl}^{NIW}) + C_{NI} = \sigma_{NI}\,A_{NI}^*(S_{tl}^{NIW}) \tag{29}$$

In case of complete wetting of the solid surface ($\phi_{sIW} = 0°$), (28) and (29) both reduce to a form similar to (15). When $\phi_{sIW} > 0°$, $A_{sI}^*(S_W^{NIW})$ and $A_{IW}^*(S_W^{NIW})$ can be determined as for the two-fluid systems with (17) and (18), respectively.

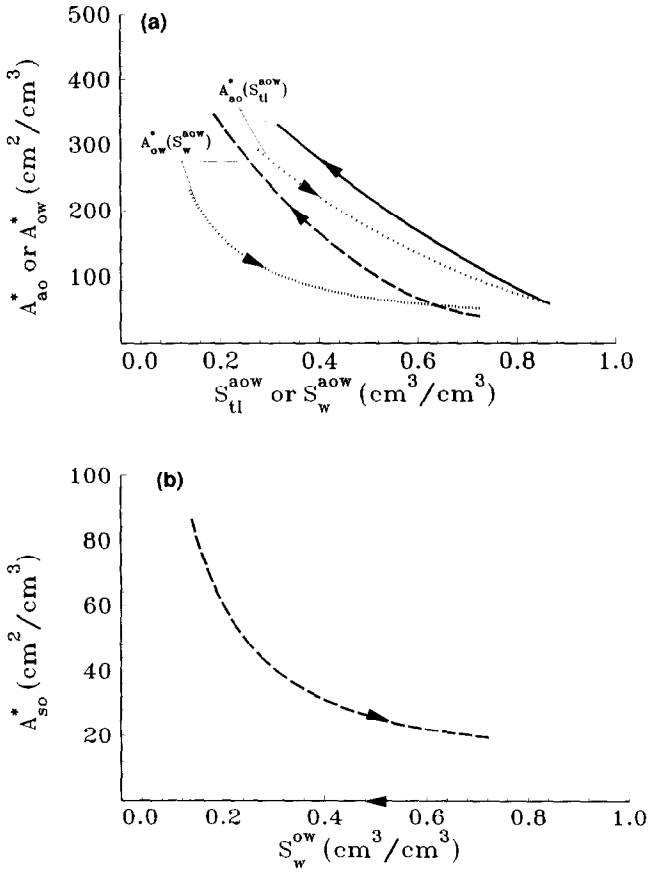

Fig. 8. Calculated three-fluid values of (a) $A_{ow}^*(S_w^{aow})$ and $A_{ao}^*(S_{tl}^{aow})$, and (b) $A_{so}^*(S_w^{aow})$ for the untreated medium which has a continuous intermediate oil phase and $\phi_{sow}^R = 0.0°$ and $\phi_{sow}^A = 51.6°$. The water saturation is varied at a constant oil saturation of 0.14.

Fig. 8a shows the calculated values of $A^*_{ao}(S^{aow}_{tl})$ and $A^*_{ow}(S^{aow}_{w})$ for the untreated medium when S^{aow}_{w} is varied at a constant S^{aow}_{o} of 0.14. This strongly water-wet medium has a continuous intermediate oil phase since oil spreads on the air–water interface ($\Sigma^*_{o/w} = +0.002$ N m^{-1}). If the $A^*_{ow}(S^{aow}_{w})$ curve for drainage is shifted to the right ($\Delta S^{aow}_{o} = 0.14$), the $A^*_{ow}(S^{aow}_{w})$ and $A^*_{ao}(S^{aow}_{tl})$ relationships for drainage match closely since oil "wets" water in a similar manner as water "wets" the solid. In contrast, the imbibition curves do not agree as well due to dissimilar "wetting" ($\phi^{A}_{sow} = 51.6°$ and $\Sigma^*_{o/w} = +0.002$ N m^{-1}). Fig. 8b shows $A^*_{so}(S^{aow}_{w})$ calculated for the untreated medium. Note that $A^*_{so}(S^{aow}_{w}) > 0$ during imbibition due to $\phi^{A}_{sow} = 51.6°$. The P_c–S curves needed to estimate interfacial areas of three-fluid media may also be estimated from data for two-fluid media using scaling and Leverett's assumption.

4.2. Discontinuous intermediate fluid

Bradford and Leij (1995a,b) found that a continuous intermediate phase was not always present in oil-wet and fractional wettability media. Six interfaces ($N_i = 6$) may exist. The possible interfaces are water–solid, oil–solid, air–solid, oil–water, air–oil, and air–water (i = sw, so, sa, ow, ao, aw). We again assume isothermal conditions and incompressibility of fluids and solid. At equilibrium δW_{ext} is equal to the work expended to change the six interfacial areas, $\Sigma \sigma_i \delta A_i$.

If the intermediate fluid is not continuous the relationship between the interfacial areas and δW_{ext} is not as easily determined as for water-wet media since three capillary pressure drops need to be considered (P_{ow}, P_{ao}, and P_{aw}). Bradford and Leij (1995b) observed that P_{ow} and P_{aw} depended mainly on S^{aow}_{w}, whereas P_{ao} was primarily a function of S^{aow}_{o}. The P_{ow}–S^{aow}_{w} relationship could be predicted directly from the measured two-fluid P_{ow}–S^{ow}_{w} data (Bradford and Leij, 1996). The two-fluid fractional wettability P_{ow}–S^{ow}_{w} relation previously discussed (cf. Fig. 6) depends on A^*_{so}, A^*_{sw}, and A^*_{ow}; values of A^*_{so} and A^*_{sw} determine the magnitude of the water- and oil-wet regions of the P_{ow}–S^{aow}_{w} curve. We therefore assumed that the three-fluid relation, P_{ow}–S^{aow}_{w}, is also determined by A^*_{so}, A^*_{sw}, and A^*_{ow} according to

$$-P_{ow}\ \delta S^{aow}_{w} = \sigma_{sw}\ \delta A^*_{sw} + \sigma_{so}\ \delta A^*_{so} + \sigma_{ow}\ \delta A^*_{ow} \tag{30}$$

The value of A^*_{ow} can be estimated by (20) and (21) if $A^*_{sa} = 0$.

Fig. 9a shows the calculated A^*_{ow} for a three-fluid OTS sand, according to (20) and (21), if S^{aow}_{w} is varied at a constant $S^{aow}_{o} = 0.15$. The capillary pressure, P_{ow}, in this "oil-wet" medium is mostly negative. Note that the value of A^*_{ow} is higher during imbibition than drainage of water (constant S^{aow}_{o}). More work is required to imbibe water since it generally acts as intermediate fluid.

Bradford and Leij (1996) found that in case S^{aow}_{o} is varied, at a constant S^{aow}_{w}, the P_{ao}–S^{aow}_{tl} relationship could be directly predicted from the P_{ao}–S^{ao}_{o} curve. On the other hand, when S^{aow}_{w} is varied at a constant S^{aow}_{o}, this P_{ao}–S^{aow}_{tl} relation could only be predicted using an additional (empirical) assumption that the value of P_{ao} changes linearly with S^{aow}_{w}. We denote S^{aow}_{tl} as $S^{aow}_{tl(o)}$ when S^{aow}_{o} changes (at a constant S^{aow}_{w}) and as $S^{aow}_{tl(w)}$ when S^{aow}_{w} changes (at a constant S^{aow}_{o}). Just as we used the two-fluid P_{ao}–S^{ao}_{o}

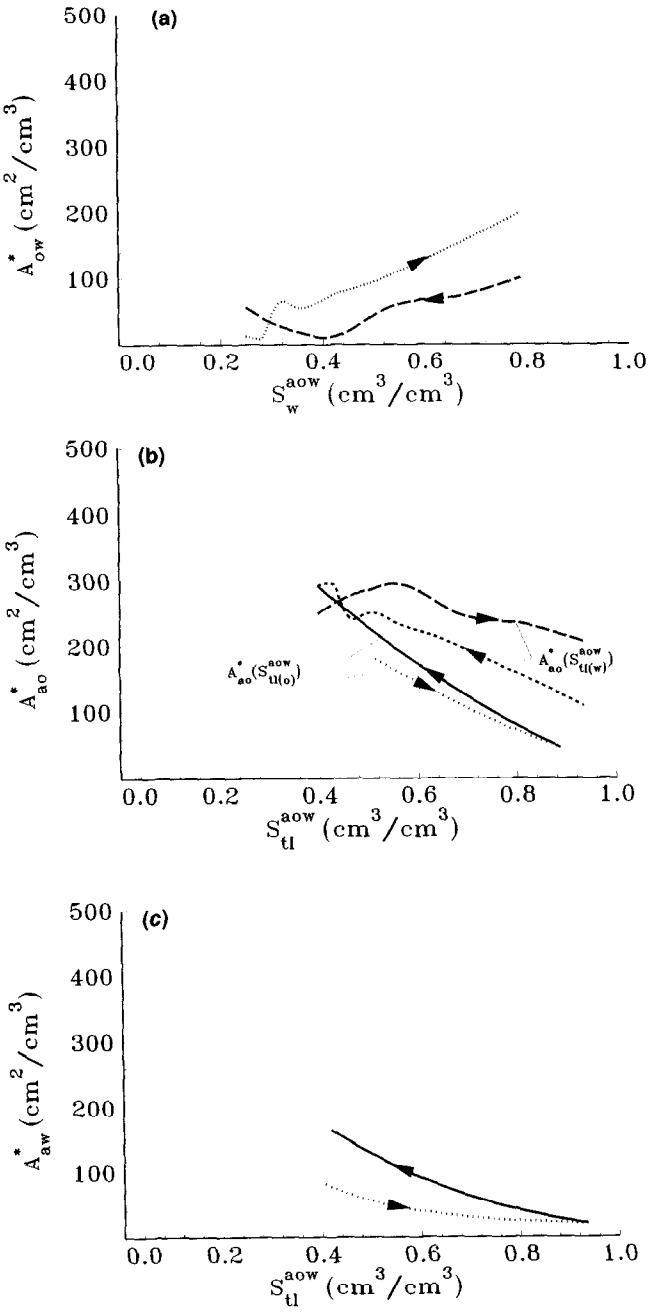

Fig. 9. The calculated values of (a) A^*_{ow}, (b) A^*_{ao}, and (c) A^*_{aw} for the 100% OTS medium. In (a), (b), and (c) S^{aow}_w is varied at a constant $S^{aow}_o = 0.15$, while in (b) S^{aow}_o is also varied at a constant $S^{aow}_w = 0.27$.

relation to predict A^*_{ao} (cf. Fig. 3) we can use the P_{ao}–$S^{aow}_{tl(o)}$ curve to predict A^*_{ao} for a three-fluid fractional wettability system (constant S^{aow}_{w}):

$$-P_{ao}\,\delta S^{aow}_{tl(o)} = \sigma_{ao}\,\delta A^*_{ao} \tag{31}$$

The value of A^*_{ao} can not be determined from the area under the P_{ao}–$S^{aow}_{tl(w)}$ curve, i.e., variable water and air saturations, since this area does not correspond to the external work required to move the air–oil interface. We estimated $A^*_{ao}(S^{aow}_{tl(w)})$ by assuming that $A^*_{ow} + A^*_{ao}$ is constant for three-fluid systems if the oil saturation is not changed:

$$A^*_{ao}\left(S^{aow}_{tl(w)}\right) = c_{ao} - A^*_{ow}\left(S^{aow}_{w}\right) \tag{32}$$

where c_{ao} is equal to the initial value of $A^*_{ao} + A^*_{ow}$, i.e., at the start of water drainage or imbibition. Fig. 9b shows the A^*_{ao} curves calculated according to (31) and (32) for the OTS medium. Note that A^*_{ao} is influenced to a greater extent by $S^{aow}_{tl(o)}$ ($S^{aow}_{w} = 0.27$) than by $S^{aow}_{tl(w)}$ ($S^{aow}_{o} = 0.15$). According to (32), the $A^*_{ao}(S^{aow}_{tl(w)})$ relationship changes primarily during water imbibition due to the previously mentioned dependency of A^*_{ow} on S^{aow}_{w}.

Finally, we consider the capillary pressure over the air–water interface to estimate A^*_{aw}. In analogy to the P_{ao}–$S^{aow}_{tl(o)}$ relationship, we postulate that the area under the P_{aw}–$S^{aow}_{tl(w)}$ curve is related to changes in A^*_{aw} as follows

$$-P_{aw}\,\delta S^{aow}_{tl(w)} = \sigma_{aw}\,\delta A^*_{aw} \tag{33}$$

The value of A^*_{aw} can not be determined from the area under the P_{aw}–$S^{aow}_{tl(o)}$ curve since this area does not correspond to the external work required to move the air–water interface. We may estimate $A^*_{aw}(S^{aow}_{tl(o)})$ by assuming that $A^*_{ow} + A^*_{aw}$ is constant since the water saturation remains constant:

$$A^*_{aw}\left(S^{aow}_{tl(o)}\right) = c_{aw} - A^*_{ow}\left(S^{aow}_{o}\right) \tag{34}$$

where c_{aw} is a constant equal to $A^*_{aw} + A^*_{ow}$ at the start of oil drainage or imbibition. Note that $A^*_{aw}(S^{aow}_{tl(o)})$ is constant since A^*_{ow} is not a function of S^{aow}_{o} (Bradford and Leij, 1995a). Fig. 9c shows $A^*_{aw}(S^{aow}_{tl(w)})$, when $S^{aow}_{o} = 0.15$, calculated according to (33) for the 100% OTS medium. At a given $S^{aow}_{tl(w)}$, A^*_{aw} is greater for drainage than for imbibition because of hysteresis in the P_{aw}–$S^{aow}_{tl(w)}$ curve. A comparison of Fig. 9a and Fig. 9c reveals that A^*_{ow} and A^*_{aw} are inversely related for changes in S^{aow}_{w}. In contrast, (34) suggests that A^*_{ow} and A^*_{aw} are mainly constant for changes in S^{aow}_{o} (constant S^{aow}_{w}) and hence A^*_{ao} is mainly affected by changes in S^{aow}_{o} (cf. Fig. 9b)

5. Summary and conclusions

The thermodynamic approach discussed by Morrow (1970) was further developed to estimate interfacial areas in multi-fluid soil systems from measured two- and three-fluid P_c–S relations for a variety of wettabilities. If the solid surface was completely wetted, the area under the P_c–S curve for two-fluid media was directly proportional to A^*_{NW}; the maximum value occurred when the wetting fluid became discontinuous (S^{NW}_{rW}). For main imbibition and drainage cycles, nonwetting fluid entrapment resulted in additional interfacial area, $A^*_{NW}(\chi)$. We estimated this additional area by assuming that the fluid

was entrapped as spheres with four saturation dependent diameters. If the solid was not completely wetted by one fluid, the values of A^*_{NW} and A^*_{sN} were deduced by weighed partitioning of the area under the P_{NW}–S^{NW}_W curve, Φ_{NW}, into two regions according to (17) and (18). Media that were strongly wetted had a greater A^*_{NW} and a lower A^*_{sN}.

For fractional wettability media, the P_{ow}–S^{ow}_w curve has water- ($P_{ow} > 0$) and oil-wet ($P_{ow} < 0$) regions. The previously discussed technique for uniform wettability media was applied separately to these regions to determine the oil–water interfacial area, $A_{ow}(S^{ow}_w)$. Estimated values of A_{ow} had local maxima at residual saturations, S^{ow}_{ro} and S^{ow}_{rw}, with a local minimum at the point of wetting reversal at $P_{ow} = 0$.

For three-fluid media the wetting and spreading behavior of the liquids dramatically affected the calculated interfacial areas. For a water-wet medium with a continuous intermediate oil phase, a similar thermodynamic description was used as for two-fluid media. The area under the $P_{ow}(S^{aow}_w)$ curve depended on A^*_{ow} and A^*_{so}, whereas the area under the $P_{ao}(S^{aow}_{tl})$ was used to predict A^*_{ao}. As many as six interfaces exist in oil-wet or fractional wettability media containing three fluids. We deduced the relationship between external work and interfacial areas from our ability to predict three-fluid P_c–S relations from two-fluid P_c–S data (Bradford and Leij, 1996). Values of $A^*_{ow}(S^{aow}_w)$, $A^*_{ao}(S^{aow}_{tl(o)})$, and $A^*_{aw}(S^{aow}_{tl(w)})$ were estimated from the three-fluid P_c–S relations in a manner similar to two-fluid systems. The values of $A^*_{ao}(S^{aow}_{tl(w)})$ and $A^*_{aw}(S^{aow}_{tl(o)})$ were determined by assuming that when S^{aow}_w changes the value of $A^*_{ow} + A^*_{ao}$ is constant and when S^{aow}_o changes the value of $A^*_{ow} + A^*_{aw}$ is constant.

Our procedures for estimating the interfacial areas of multi-fluid soil systems may lead to a better understanding of many flow and transport processes. However, the estimation procedure is based on a number of assumptions that need further investigation. We assumed equilibrium isothermal conditions, constant solid surface area, a macroscopic extension of Young's equation, and incompressibility of fluid and solid phases. There is an obvious need to assess the estimation procedure with direct measurement techniques. Procedures should soon become available for measuring interfacial areas of multi-fluid systems such as those discussed here.

6. Notation

a	air
A_i	interfacial area of interface i (cm^2)
A_{kl}	interfacial area between phases k and l (cm^2)
A^*_{kl}	interfacial area per unit pore volume between phases k and l ($cm^2\ cm^{-3}$)
A_s	surface area (cm^2)
A^*_s	surface area per unit pore volume ($cm^2\ cm^{-3}$)
c_{ao}	value of $A^*_{ow} + A^*_{ao}$ at the start of water drainage or imbibition ($cm^2\ cm^{-3}$)
c_{aw}	value of $A^*_{ow} + A^*_{aw}$ at the start of oil drainage or imbibition ($cm^2\ cm^{-3}$)
C_o	constant due to entrapped oil in fractional wettability media ($N\ m^{-2}$)
C_w	constant due to entrapped water in fractional wettability media ($N\ m^{-2}$)
C_{kl}	constant due to nonwetting fluid entrapment in k and l system ($N\ m^{-2}$)
d	denser fluid

E	total energy (N m)
f	weighing function
F	Helmholtz free energy (N m)
F_o	fraction of total solid surface area which is oil-wet
i	interface
j	index
I	intermediate wetting fluid
l	lighter fluid
n	parameter (slope of inflection point) for van Genuchten P_c–S model
N	nonwetting fluid
N_i	number of interfaces
N_p	number of phases
o	oil
OTS	octadecyltrichlorosilane
p	phase
P_c	capillary pressure (N m^{-2}, cm water)
P_p	pressure of phase p (N m^{-2}, cm water)
P_{kl}	capillary pressure drop over interface between fluids k and l, i.e., $P_k - P_l$ (N m^{-2}, cm water)
r^2	regression coefficient for the goodness of fit
q	heat flowing into or away from system (N m)
R	radius of a sphere or capillary tube (cm)
R_j	radius of saturation-dependent sphere j
s	solid
S	saturation (cm^3 cm^{-3})
S_k^{kl}	saturation of fluid k in a medium containing the two fluids k and l (cm^3 cm^{-3})
S_k^{klm}	saturation of fluid k in a medium containing the three fluids k, l, and m (cm^3 cm^{-3})
S_r	residual saturation (cm^3 cm^{-3})
$S_{tl(o)}^{aow}$	total liquid saturation when S_o^{aow} is varied at a constant S_w^{aow} (cm^3 cm^{-3})
$S_{tl(w)}^{aow}$	total liquid saturation when S_w^{aow} is varied at a constant S_o^{aow} (cm^3 cm^{-3})
$\bar{S}$	effective saturation equal to $(S - S_{rW})/(1 - S_{rW} - S_{rN})$ (cm^3 cm^{-3})
T	temperature (K)
V_b	bulk volume (cm^3)
V_p	volume of phase p (cm^3)
VTS	vinyltriethoxysilane
w	water
W	wetting fluid
W_{ext}	external work (N m)
W_{i+p}	work to changes in interfacial areas and compression (N m)
α	parameter (entry pressure) in van Genuchten P_c–S model (cm^{-1})
ε	porosity
ρ_b	bulk density (g cm^{-3})
ρ_s	specific density of the sand (g cm^{-3})
$\Sigma_{k/l}$	coefficient for spreading of fluid k on fluid l (N m^{-1})

$\Sigma^{c}_{k/l}$ contaminated coefficient for spreading (uses σ^{*}_{aw}) of fluid k on fluid l (N m^{-1})
σ^{c}_{aw} contaminated air–water interfacial tension (N m^{-1})
σ_i interfacial tension of interface i (N m^{-1})
σ_{kl} interfacial tension at interface between fluids k and l (N m^{-1})
Φ_{kl} area under the P_c–S curve determined by fluids k and l (N m^{-2})
ϕ_{skl} equilibrium contact angle at contact line between solid and fluids i and j (deg)
ϕ^{A}_{skl} advancing contact angle (deg)
ϕ^{R}_{skl} receding contact angle (deg)
λ parameter (for shifting) the modified van Genuchten P_c–S model (cm water)
Λ entropy (N m K^{-1})
χ value of S^{ow}_{w} when $P_{ow} = 0$ (χ_{MD} main drainage; χ_{MI} main imbibition) (cm^3 cm^{-3})

Acknowledgements

This study was funded in part by a grant from the Kearney Foundation of Soil Science. We thank Mr. Jim Wood and Dr. Donald Suarez for their help with measuring the solid surface area.

References

Adamson, A.W., 1990. Physical Chemistry of Surfaces, 5th edition. John Wiley and Sons Inc, New York, p. 570.

Anbeek, C., 1993. The effect of natural weathering on dissolution rates. Geochim. Cosmochim. Acta 57, 4963–4975.

Anderson, R., Larson G., Smith, C., 1991. Silicon Compounds: Register and Review, 5th Edition. Huls America Inc., Piscataway, NJ.

Bradford, S.A., Leij, F.J., 1995a. Wettability effects on scaling two- and three-fluid capillary pressure–saturation relations. Environ. Sci. Technol. 29, 1446–1455.

Bradford, S.A., Leij, F.J., 1995b. Fractional wettability effects on two- and three-fluid capillary pressure–saturation relations. J. Contam. Hydrol. 20, 89–109.

Bradford, S.A., Leij, F.J., 1996. Predicting two- and three-fluid capillary pressure–saturation relations in fractional wettability media. Water Resour. Res. 32, 251–260.

Brown, R.J.S., Fatt, I., 1956. Measurements of fractional wettability of oilfield rocks by the nuclear magnetic relaxation method. Trans. Am. Inst. Mineral. Metall. Petrol. Eng. 207, 262–264.

Brunauer, S.L., Emmett, P.H., Teller, E., 1938. Adsorption of gases in multi-molecular layers. J. Am. Chem. Soc. 60, 309.

Cary, J.W., 1994. Estimating the surface area of fluid phase interfaces in porous media. J. Contam. Hydrol. 15, 243–248.

Chatzis, I., Morrow N.R., Lim, H.T., 1983. Magnitude and detailed structure of residual oil saturation. Soc. Petrol. Eng. J. (April), 311–326.

Collins, R.E., 1961. Flow of fluids through porous materials. Reinhold, New York, NY.

Corey, A.T., 1986. Mechanics of immiscible fluids in porous media. Water Resour. Public., Highlands Ranch, CO.

du Noüy, P.L., 1919. A new apparatus for measuring surface tension. J. Gen. Physiol. 1, 521–524.

Ferrand, L.A., Milly, P.C.D., Pinder G.F., Turrin, R.P., 1990. A comparison of capillary pressure–saturation relations for drainage in two- and three-fluid porous media. Adv. Water Resour. 13, 54–63.

Gibbs, J.W., 1961. Scientific papers, vol. 1. Dover, New York, NY, pp. 219–331.

Gvirtzman, H., Roberts, P.V., 1991. Pore scale spatial analysis of two immiscible fluids in porous media. Water Resour. Res. 27, 1165–1176.

Hassanizadeh, S.M., Gray, W.G., 1993. Thermodynamic basis of capillary pressure in porous media. Water Resour. Res. 29, 3389–3406.

Herman, B., Lemasters, J.J., 1993. Optical Microscopy: Emerging Methods and Applications. Academic Press, New York, NY.

Klute, A., 1986. Water Retention: Laboratory Methods. In: Klute A. (Ed.), Methods of Soil Analysis, part 1. ASA, SSSA, Madison, WI, pp. 635–662.

Lenhard, R.J., Parker, J.C., 1988. Experimental validation of the theory of extending two-phase saturation–pressure relations to three-fluid phase systems for monotonic drainage paths. Water Resour. Res. 24, 373–380.

Leverett, M.C., 1941. Capillary behavior in porous solids. Trans. Am. Inst. Mineral. Metall. Petrol. Eng. 142, 152–169.

Melrose, J.C., 1965. Wettability as related to capillary action in porous media, Soc. Petrol. Eng. J. (September), 259–271.

Miller, C.T., Poirier-McNeill M.M., Mayer, A.S., 1990. Dissolution of trapped nonaqueous phase liquids: mass transfer characteristics. Water Resour. Res. 26, 2783–2796.

Montemagno, C.D., Gray, W.G., 1995. Photoluminescent volumetric imaging: a technique for the exploration of multiphase flow and transport in porous media. Geophys. Res. Lett., 22, 425–428.

Morrow, N.R., 1970. Flow through porous media, In: de Wiest, R.J.M. (Ed.), Physics and Thermodynamics of Capillary Action in Porous Media. Academic Press, New York.

Morrow, N.R., 1976. Capillary pressure correlations for uniformly wetted porous media. J. Can. Petrol. Technol. (Oct–Dec), 49–69.

Payne, D., 1953. A method for the determination of the approximate surface area of particulate solids. Nature 172, 261.

Pfannkuch, H.O., 1984. Ground-water contamination by crude oil at the Bemidji, MN, research site: US Geological Survey Toxic Waste—Ground-Water Contamination Study, paper presented at Toxic-Waste Technical Meeting, US Geol. Surv., Reston, VA.

Powers, S.E., Abriola L.M., Weber, W.J., Jr., 1992. An experimental investigation of NAPL dissolution in saturated subsurface systems: steady state mass transfer rates. Water Resour. Res. 28, 2691–2705.

Rapoport, L.A., Leas, W.J., 1951. Relative permeability to liquid in liquid–gas systems. Trans. Am. Inst. Mineral. Metall. Petrol. Eng. 192, 83–95.

Ronen, D., Margarite, M., Paldor N., Bachmat, Y., 1986. The behavior of groundwater in the vicinity of water table. Water Resour. Res. 22, 1217–1224.

Saripalli, K.P., Rao P.S.C., Annable, M.D., 1995. Use of interfacial tracers for characterization of non-aqueous phase liquids (NAPL) in the sub-surface. EOS (Suppl.), Am. Geophys. Union 76 (17), S123.

Streile, G.P., Cary J.W., Fredrickson, J.K., 1991. Innocuous oil and small thermal gradient for in situ remediation. In: Proceedings of National Research and Development Conference on the Control of Hazardous Materials, Anaheim, CA. Hazardous Materials Control Res. Inst., Pasadena, CA, pp. 32–37.

van Genuchten, M.Th., 1980. A closed form equation for predicting the hydraulic conductivity of unsaturated soils. Soil Sci. Soc. Am. J. 44, 892–898.

Wan, J., Wilson, J.L., 1994. Colloid transport in unsaturated porous media. Water Resour. Res. 30, 857–864.

Wiesendanger, R., 1994. Scanning Probe Microscopy and Spectroscopy: Methods and Applications. Cambridge University Press, New York, NY.